Single-Crystal X-ray Structure Determination of Tris(pyrazol-1-yl)methane Triphenylphosphine Copper(I) Tetrafluoroborate, Hirshfeld Surface Analysis and DFT Calculations

Jesús Castro [1], Valentina Ferraro [2] and Marco Bortoluzzi [2,3,*]

[1] Departamento de Química Inorgánica, Universidade de Vigo, Facultade de Química, Edificio de Ciencias Experimentais, 36310 Vigo, Galicia, Spain; jesusc@uvigo.gal
[2] Dipartimento di Scienze Molecolari e Nanosistemi, Università Ca' Foscari Venezia, 30172 Mestre, Italy; valentina.ferraro@unive.it
[3] CIRCC, via Celso Ulpiani 27, 70126 Bari, Italy
* Correspondence: markos@unive.it; Tel.: +39-0412348651

Abstract: The tetrafluoroborate salt of the cationic Cu(I) complex $[Cu(CHpz_3)(PPh_3)]^+$, where $CHpz_3$ is the tridentate N-donor ligand tris(pyrazol-1-yl)methane and PPh_3 is triphenylphosphine, was synthesized through a displacement reaction on the acetonitrile complex $[Cu(NCCH_3)_4][BF_4]$. The compound crystallizes in the monoclinic $P2_1/c$ space group. The single-crystal X-ray diffraction revealed that the copper(I) centre is tetracoordinated, with a disposition of the donor atoms surrounding the metal centre quite far from the ideal tetrahedral geometry, as confirmed by continuous shape measures and by the τ_4 parameter. The intermolecular interactions at the solid state were investigated through the Hirshfeld surface analysis, which highlighted the presence of several non-classical hydrogen bonds involving the tetrafluoroborate anion. The electronic structure of the crystal was modelled using plane-wave DFT methods. The computed band gap is around 2.8 eV and separates a metal-centred valence band from a ligand-centred conduction band. NMR spectroscopy indicated the fluxional behaviour of the complex in $CDCl_3$ solution. The geometry of the compound in the presence of chloroform as implicit solvent was simulated by means of DFT calculations, together with possible mechanisms related to the fluxionality. The reversible dissociation of one of the pyrazole rings from the Cu(I) coordination sphere resulted in an accessible process.

Keywords: copper(I); tris(pyrazol-1-yl)methane; triphenylphosphine; single-crystal X-ray diffraction; Hirshfeld surface analysis; DFT calculations

1. Introduction

Tris(pyrazol-1-yl)alkanes constitute a family of tridentate N-donor ligands widely employed in coordination chemistry, homogeneous catalysis and bioinorganic chemistry [1–11], where tris(pyrazol-1-yl)methane ($CHpz_3$) represents the simplest compound. $CHpz_3$ and the related homoleptic Fe(II) complex were first reported in 1979 by Mani [12]. Being isoelectronic with the anion tris(pyrazol-1-yl)borate, $CHpz_3$ is generally considered a C-scorpionate.

In recent years, particular interest was devoted to the preparation of copper tris(pyrazol-1-yl)alkane complexes [13,14]. The first Cu(II) derivatives were reported in 1985, having general formulae $[Cu(CHpz_3)X_2]$ (X = Cl, Br, CH_3COO) and $[Cu(CHpz_3)_2]X_2$ (X = Cl, Br, NO_3, ClO_4) [15]. The chemistry of tris(pyrazol-1-yl)alkanes with Cu(I) started in 1996, with the isolation of cationic carbonyl and acetonitrile complexes with substituted tris(pyrazol-1-yl)alkane ligands having the formulae $[Cu(CH^{R,R'}pz_3)(CO)][PF_6]$ and $[Cu(CH^{R,R'}pz_3)(NCCH_3)][PF_6]$ ($CH^{R,R'}pz_3$ = tris(3,5-dimethylpyrazol-1-yl)methane, tris(3-phenylpyrazol-1-yl)methane and tris(3-*tert*-butylpyrazol-1-yl)methane) [16]. In the case of Cu(II) deriva-

tives, the coordination number generally varies from five to six [17], while most of the Cu(I) are four coordinated, with the C-scorpionate acting as κ^3-ligand and the fourth coordination site occupied by a monodentate ligand. Besides acetonitrile, several other nitrogen donors were successfully coordinated, for instance, cyanamides [18], six-membered N-donor heterocycles [19], NO radical [20] and nitrite [21]. Instead of CO, electronically related isocyanides can also occupy the fourth position of the Cu(I) coordination sphere [22].

Cu(I) complexes with tris(pyrazol-1-yl)alkanes and a monodentate phosphine were reported in the literature and investigated in selected cases for applications in medicinal chemistry [23–26]. The tris(pyrazol-1-yl)alkanes considered are, besides $CHpz_3$, tris(3,5-diisopropyl-1-pyrazolyl)methane, tris(pyrazol-1-yl)methanesulfonate and tris(3-phenylpyrazol-1-yl)methanesulfonate, while the phosphines are triphenylphosphine (PPh_3), tris(*m*-sulfonatophenyl)phosphine, tris(cyanoethyl)phosphine, 1,3,5-triaza-7-phosphaadamantane and its N-methylated derivative. Quite surprisingly, the simplest $CHpz_3$ C-scorpionate was mainly used in combination with 1,3,5-triaza-7-phosphaadamantane and tris(cyanoethyl) phosphine. The X-ray structures of the hexafluorophosphate and nitrate salts of $[Cu(CHpz_3) (PPh_3)]^+$ are, however, present in the Cambridge Crystallographic Data Centre (CCDC 234259 and 246420) [27,28]. The related $[Cu(CHbtz_3)(PPh_3)][BF_4]$ complex, where $CHbtz_3$ is tris(benzotriazol-1-yl)methane, was recently reported by our research group together with the single-crystal X-ray structure determination of $CHbtz_3$ [29]. Given our interest towards the preparation of Cu(I) coordination compounds with polydentate azole-based ligands [30,31], in this paper, we report the synthesis, characterization and single-crystal X-ray structure determination of $[Cu(CHpz_3)(PPh_3)][BF_4]$. The supramolecular network was studied employing the Hirshfeld surface determination, while selected aspects of the compound in the solid state and in solution were investigated by means of DFT calculations.

2. Experimental Section

2.1. Materials and Methods

Commercial solvents (Merck, Darmstadt, Germany) were purified as described in the literature [32]. Cu_2O, $HBF_4 \cdot Et_2O$ and the organic reactants were purchased from Alfa Aesar (Ward Hill, MA, USA) and Merck (Darmstadt, Germany) and used as received. The acetonitrile complex $[Cu(NCCH_3)_4][BF_4]$ was synthesized following a reported procedure [33]. Tris(pyrazol-1-yl)methane $CHpz_3$ was prepared employing common Schlenk techniques according to a published method [34]. The reactions involving Cu(I) were carried out under inert atmosphere, working in a MBraun (Garching, Germany) Labstar glove box with MB 10G gas purifier filled with N_2 and equipped for inorganic syntheses.

Elemental analyses (C, H, N) were carried out using an Elementar (Langenselbold, Germany) Unicube microanalyzer. Conductivity measurements were carried out at 298 K using an XS Instruments (Modena, Italy) Cond 80+ conductometer. Melting points were registered using a FALC (Bergamo, Italy) 360 D instrument equipped with a camera. Nuclear magnetic resonance (NMR) spectra were collected at variable temperatures employing a Bruker (Billerica, MA, USA) Avance 400 instrument operating at 400.13 MHz of ^{1}H resonance. ^{1}H NMR spectra are referred to the partially non-deuterated fraction of the solvent, itself referred to tetramethylsilane. $^{31}P\{^1H\}$ NMR resonances are referred to 85% H_3PO_4 in water. $^{19}F\{^1H\}$ NMR resonances are referred to $CFCl_3$.

2.2. Synthesis of $[Cu(CHpz_3)(PPh_3)][BF_4]$

$[Cu(NCCH_3)_4][BF_4]$ (0.478 g, 1.5 mmol) was dissolved under N_2 in 20 mL of dry dichloromethane inside the glove box. A stoichiometric amount of PPh_3 (0.393 g, 1.5 mmol) was added to the solution, and the reaction mixture was stirred at room temperature for four hours. $CHpz_3$ (0.321 g, 1.5 mmol) was then added, and the solution was stirred overnight at room temperature. The solvent was evaporated under reduced pressure, and diethyl ether (10 mL) was added. The white solid that separated was collected by filtration, washed two times with 5 mL of diethyl ether and dried under vacuum. Yield 0.583 g (62%).

Crystals suitable for X-ray diffraction were grown by means of slow diffusion of diethyl ether in dichloromethane solutions.

Characterization of [Cu(CHpz$_3$)(PPh$_3$)][BF$_4$]. Anal. calcd for C$_{28}$H$_{25}$BCuF$_4$N$_6$P (626.86 g mol^{-1}, %): C, 53.65; H, 4.02; N, 13.41. Found (%): C, 53,45; H, 4.04; N, 13.39. M.p. (°C): 196. Λ_M (acetone, ohm^{-1}mol^{-1}cm^2): 142. ^{1}H NMR (CDCl$_3$, 300 K): δ 9.44 (s, 1H, CH), 8.43 (d, 3H, J_{HH} = 2.8 Hz, Pz), 7.65–7.40 (m, 15H, PPh$_3$), 7.32 (d, 3H, J_{HH} = 1.9 Hz, Pz), 6.32 (d, 3H, J_{HH} = 2.8 Hz, J_{HH} = 1.9 Hz, Pz). ^{31}P{^{1}H} NMR (CDCl$_3$, 300 K): δ 8.63 (FWHM = 250 Hz). ^{19}F{^{1}H} NMR (CDCl$_3$, 300 K): −149.79 (^{10}B-F), −149.84 (^{11}B-F).

2.3. Crystal Structure Determination and Hirshfeld Surface Analysis

Crystallographic data were collected at CACTI (Universidade de Vigo) using a Bruker (Billerica, MA, USA) D8 Venture Photon II CMOS detector and Mo-Kα radiation (λ = 0.71073 Å) generated by an Incoatec (Geesthacht, Germany) Microfocus Source IμS. The temperature was kept at 100 K employing an Oxford Cryosystems (Oxford, UK) Crystream 800 cooler. The software APEX3 version 2019-11-0 [35] was used for collecting frames of data, indexing reflections and determining lattice parameters; SAINT version 8.40B for integration of intensity of reflections [35] and SADABS version 2016/2 [35] for scaling and empirical absorption correction. The crystallographic treatment was performed with the Oscail version 4.7.1 (2014) program [36] and solved using the SHELXT version 2018/2 program [37]. The structure was subsequently refined by a full-matrix least-squares based on F^2 using the SHELXL version 2018/3 program [38]. Non-hydrogen atoms were refined with anisotropic displacement parameters. Hydrogen atoms were included in idealized positions and refined with isotropic displacement parameters. Other details concerning crystal data and structural refinement are given in Table 1. CCDC 2323499 contains the supplementary crystallographic data. These data can be obtained free of charge from the Cambridge Crystallographic Data Centre via www.ccdc.cam.ac.uk/structures (accessed on 26 January 2024). PLATON (version 110423) was used to obtain some geometrical parameters from the cif file [39]. Figures were drawn using Mercury version 2023.3.0 [40].

Table 1. Crystal data and structure refinement for [Cu(CHpz$_3$)(PPh$_3$)][BF$_4$].

CCDC code	2323499
Empirical formula	C$_{28}$H$_{25}$BCuF$_4$N$_6$P
Moiety formula	C$_{28}$H$_{25}$CuN$_6$P, BF$_4$
Formula weight	626.86
Temperature	100(2) K
Wavelength	0.71073 Å
Crystal system	Monoclinic
Space group	$P2_1/c$
Unit cell dimensions	a = 11.9442(9) Å
	b = 15.5313(9) Å
	c = 15.9059(12) Å
	β = 105.945(3)°
Volume	2837.2(3) Å^3
Z	4
Density (calculated)	1.468 Mg/m^3
Absorption coefficient	0.882 mm^{-1}
$F(000)$	1280
Crystal size	0.273 × 0.251 × 0.219 mm
Theta range for data collection	2.623 to 28.282°
Index ranges	$-15 \leq h \leq 13$
	$-20 \leq k \leq 20$
	$-21 \leq l \leq 21$
Reflections collected	80174
Independent reflections	7023 [R_{int} = 0.0322]
Reflections observed (>2σ)	6568
Data Completeness	0.999

Table 1. *Cont.*

Absorption correction	Semi-empirical from equivalents
Max. and min. transmission	0.7457 and 0.6079
Refinement method	Full-matrix least-squares on F^2
Data/restraints/parameters	7023/0/370
Goodness-of-fit on F^2	1.062
Final R indices [$I > 2\sigma(I)$]	$R_1 = 0.0272$
	$wR_2 = 0.0667$
R indices (all data)	$R_1 = 0.0297$
	$wR_2 = 0.0680$
Largest diff. peak and hole	0.761 and -0.485 e.Å^{-3}

The Hirshfeld surfaces were calculated using the Crystal Explorer version 3.1 program package, and the 2D fingerprint was prepared using the same software [41,42]. The deposited cif file was used as input file for the calculations. All (d_i, d_e) contacts were also expressed in the form of two-dimensional plots, known as 2D fingerprint plots [43].

2.4. Computational Details

Calculations on the crystal were carried out with the PBEsol DFT functional [44] in combination with on-the-fly generated norm-conserving pseudopotentials [45]. The plane-wave basis set cut-off was set at 1210 eV. The dispersion corrections from Tkatchenko and Scheffler were added [46]. Relativistic effects were accounted through the scalar Koelling–Harmon approximation [47]. The lattice parameters and the atomic positions were taken from the cif file and left unchanged. The cell content considered in the calculation was composed of four [Cu(CHpz$_3$)(PPh$_3$)]$^+$ cations and four [BF$_4$]$^-$ anions, corresponding to 856 explicit electrons. The charge was set to zero, and the system was treated as non-spin polarized. The software used was CASTEP 20.1 [48–50], and the 3D plots were generated with XCrysDen 1.6 [51,52].

Geometry optimizations and surface scans were carried out without symmetry constraints using the r^2-SCAN-3c method [53] based on the meta-GGA r^{2}SCAN functional [54] combined with a tailor-made triple-ζ gaussian atomic orbital basis set with refitted D4 and geometrical counter-poise corrections for London dispersion and basis set superposition error [55–57]. The C-PCM implicit solvation model was added to the calculations, considering chloroform as a continuous medium [58,59]. Calculations were carried out using ORCA 5.0.3 [60,61]. The Cartesian coordinates of the DFT-optimized geometry are provided in Supplementary Materials, Table S1.

3. Results and Discussion

3.1. Synthesis and Single-Crystal X-ray Structure Determination

[Cu(CHpz$_3$)(PPh$_3$)][BF$_4$] was synthesized under mild conditions via the stepwise addition of stoichiometric amounts of PPh$_3$ and CHpz$_3$ to a dichloromethane solution of the precursor [Cu(NCCH$_3$)$_4$][BF$_4$]. The elemental analysis data agree with the proposed formula, and the conductivity measurements revealed that the compound behaves as a 1:1 electrolyte in acetone solution [62].

[Cu(CHpz$_3$)(PPh$_3$)][BF$_4$] crystallizes in the $P2_1/c$ space group. The asymmetric unit is shown in Figure 1. Selected bond lengths and angles are summarized in the caption of Figure 1. Similarly to the hexafluorophosphate [27] or the nitrate salts [28], the complex cation is constituted by a tetracoordinated copper atom coordinated to the N,N′,N″-tridentate CHpz$_3$ ligand and PPh$_3$ as P-monodentate ligand. The geometry exhibits severe distortions, and it is best described as a vacant trigonal bipyramid rather than a tetrahedron according to the Continuous Shape Measures given in Table 2 [63,64]. The classical parameter used for tetracoordination, τ_4, is around 0.67, in line with a highly distorted trigonal bipyramid geometry (ideal values: 0.00 for planar, 1.00 for tetrahedral, 0.85 for trigonal

bipyramid) [65,66]. Continuous Shape Measures and τ_4 values for the $[Cu(CHpz_3)(PPh_3)]^+$ cation as tetrafluoroborate, hexafluorophosphate and nitrate salt are compared in Table 2.
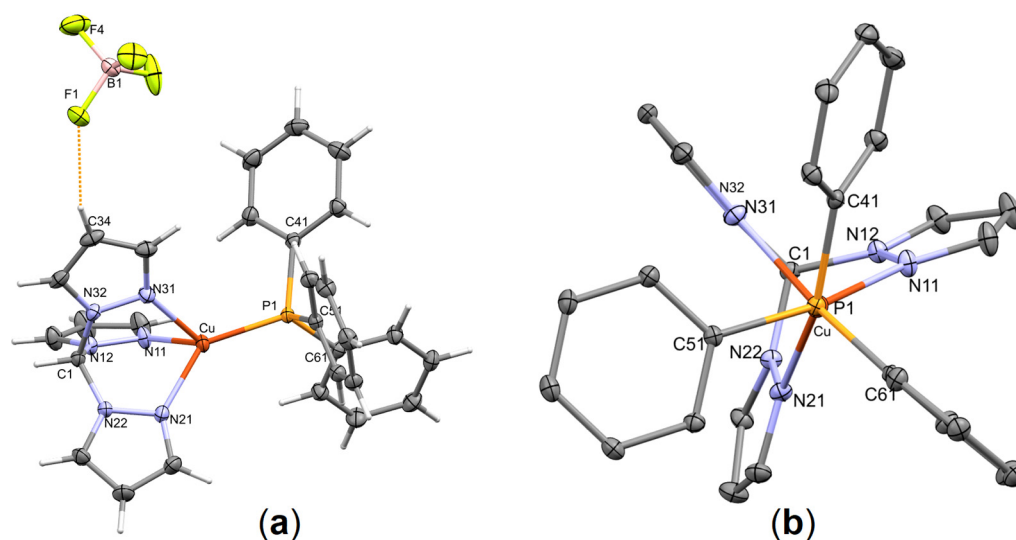

Figure 1. (**a**) Asymmetric unit of $[Cu(CHpz_3)(PPh_3)][BF_4]$. Selected bond lengths [Å] and angles [°]: Cu-N(11), 2.0863(12); Cu-N(21), 2.0477(12); Cu-N(31), 2.1144(12); Cu-P(1), 2.1541(4); N(11)-Cu-N(21), 87.08(5); N(11)-Cu-N(31), 86.10(5); N(21)-Cu-N(31), 89.64(5); N(11)-Cu-P(1), 131.38(3); N(21)-Cu-P(1), 134.20(3); N(31)-Cu-P(1), 113.25(3); C(41)-P(1)-C(51), 104.81(6); C(41)-P(1)-C(61), 105.45(6); C(51)-P(1)-C(61), 104.37(6); C(41)-P(1)-Cu, 111.46(4); C(51)-P(1)-Cu, 112.18(4); C(61)-P(1)-Cu, 117.52(4); (**b**) The $[Cu(CHpz_3)(PPh_3)]^+$ cation drawn along the Cu-P bond vector, without hydrogen atoms.

Table 2. Continuous Shape Measures and τ_4 parameter for the $[Cu(CHpz_3)(PPh_3)]^+$ cation as tetrafluoroborate, hexafluorophosphate and nitrate salt.

Anion	SP-4 [1]	T-4 [2]	SS-4 [3]	vTBPY-4 [4]	τ_4
$[BF_4]^-$	32.393	4.329	7.120	3.887	0.67
$[PF_6]^-$	31.757	4.288	6.741	3.937	0.67
$[NO_3]^-$	32.431	4.173	6.885	4.702	0.72

[1] SP-4: D_4h, Square. [2] T-4: T_d, Tetrahedron. [3] SS-4: C_{2v}, Seesaw. [4] vTBPY-4: C_{3v}, Vacant trigonal bipyramid.

Following this geometric model, the equatorial sites are occupied by two nitrogen atoms [N(11) and N(21)] of $CHpz_3$ and the phosphorus atom, P(1), of PPh_3. The axial position is filled by another nitrogen atom of $CHpz_3$, N(31), and as expected, the Cu-N bond length, equal to 2.1144(12) Å, is longer than those related to the equatorial sites, 2.0863(12) and 2.0477(12) Å long. The P(1)-Cu-N(11) and the P(1)-Cu-N(21) angles are 131.38(3) and 134.20(3)°. The third equatorial angle N(11)-Cu-N(21), equal to 87.08(5)°, is restricted by the structural rigidity of the C-scorpionate ligand. These three angles sum up to 352.7°, which is far from the 360° expected for a perfect geometry. The angle P(1)-Cu-N(31), equal to 113.25(3)°, is also far from the ideal 90° because of the rigidity of $CHpz_3$, with the N-Cu-N angles between 86.10(5) and 89.64(5)°. In the related hexafluorophosphate salt [27], the same effect can be found, although the values of the bond distances are slightly longer. On the other hand, the nitrate derivative has a more regular arrangement around the Cu(I) centre and a quasi-tetrahedral conformation [28]. Figure 1b shows the $[Cu(CHpz_3)(PPh_3)]^+$ cation drawn perpendicular to the Cu-P bond vector. It is evident that the carbon labelled as C(1) is out of the vector, with a P(1)-Cu(1)-C(1) angle of 166.03(3)°. A similar value was found for the PF_6^- derivative, but in the NO_3^- salt, the angle was 172.9°. The main difference among these compounds is the relative disposition of the pyrazolyl and phenyl rings since they are eclipsed in the nitrate salt but staggered both in the hexafluorophosphate salt and in the title compound (see also Figure S1). These differences also generate a different network

since, in the nitrate salt, the interactions between molecules are due to CH···π interactions, while in [Cu(CHpz$_3$)(PPh$_3$)][BF$_4$], the supramolecular network is mainly governed by the presence of the anion, being the fluorine atoms H-acceptors of non-classical hydrogen bonds. All the fluorine atoms of the BF$_4^-$ anion are implicated in at least one interaction, whose parameters are set out in Table 3. The non-classical hydrogen bonds are represented in Figure 2.

Table 3. Hydrogen bond parameters for [Cu(CHpz$_3$)(PPh$_3$)][BF$_4$] [Å and °].

D-H...A	d(D-H)	d(H...A)	d(D...A)	<(DHA)
C(34)-H(34)...F(1)	0.95	2.27	3.1367(18)	151.6
C(1)-H(1)...F(1 ^{i})	1.00	2.26	3.1381(16)	146.5
C(13)-H(13)...F(1 ^{i})	0.95	2.42	3.1223(19)	130.7
C(25)-H(25)...F(2 ^{ii})	0.95	2.36	3.3073(17)	174.7
C(14)-H(14)...F(3 ^{iii})	0.95	2.49	3.342(2)	149.0
C(23)-H(23)...F(4 ^{i})	0.95	2.53	3.2634(19)	133.9
C(1)-H(1)...F(4 ^{i})	1.00	2.45	3.3596(18)	150.4

Symmetry operations: ^{i} 1 − x, 1 − y, 2 − z; ^{ii} x − 1, 1/2 − y, z − 1/2; ^{iii} 1 − x, y + 1/2, 3/2 − z.
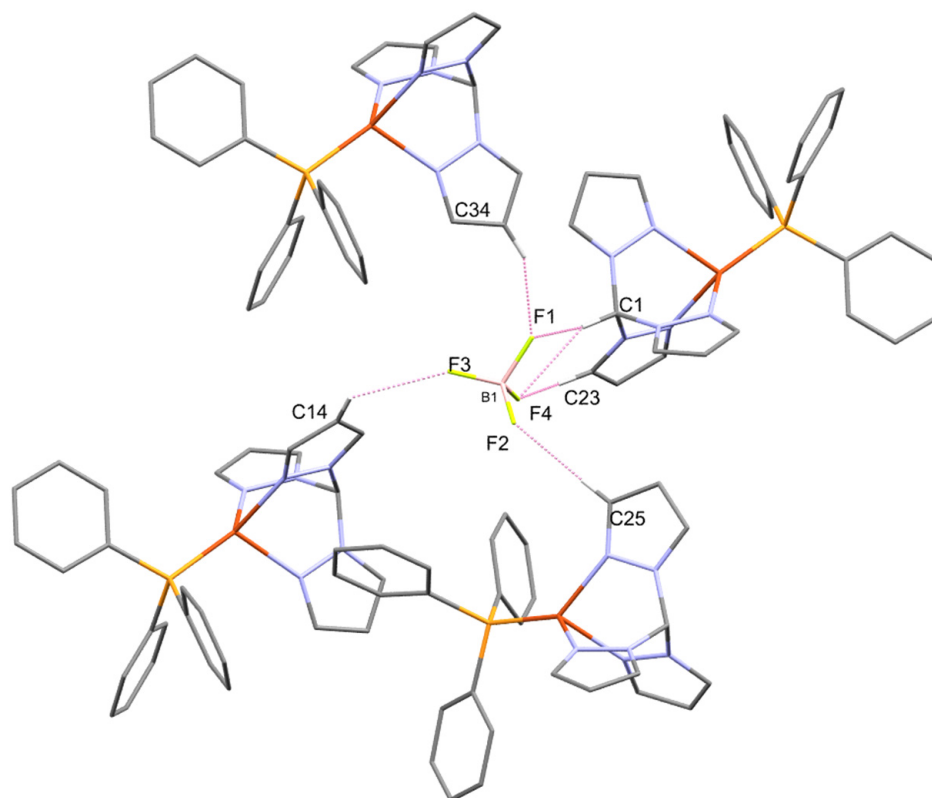

Figure 2. Non-classical hydrogen bonds in [Cu(CHpz$_3$)(PPh$_3$)][BF$_4$]. Colour map: Cu, reddish-orange; P, orange; F, greenish yellow; N, blue; C, green; B, pink; H, white. Only the hydrogen atoms involved in hydrogen bonds are drawn.

3.2. Hirshfeld Surface Analysis and Plane-Wave DFT Calculations

With the aim of deepening the knowledge about the supramolecular network, the Hirshfeld surface analysis was carried out. This technique allows for the investigation of the interactions in crystal structures through the visual recognition of several properties of intermolecular interactions (curvedness, shape index, d$_{norm}$, etc.) mapped onto proper surfaces. The surfaces were drawn in this paper by the representation of the normalized contact distance, d$_{norm}$, defined as the sum of d$_i$ (the distance of the point from the nearest nucleus within the surface) and d$_e$ (the distance of the point from the nearest nucleus

outside the surface) normalised by the van der Waals radius of the atom involved [41]. The transparent surfaces shown in Figure 3 were calculated only for the cation to show the interactions with BF_4^- and are mapped over a d_{norm} range between -0.31 and 1.54 Å. The deep red spots visible on the d_{norm} surfaces are indicative of non-classical hydrogen-bonding contacts, most of them representing interactions with symmetry-related anions found in the network [67]. Related surfaces with other mapped quantities (d_i, d_e, curvedness and shape index) are collected in Supplementary Materials, Figure S2.
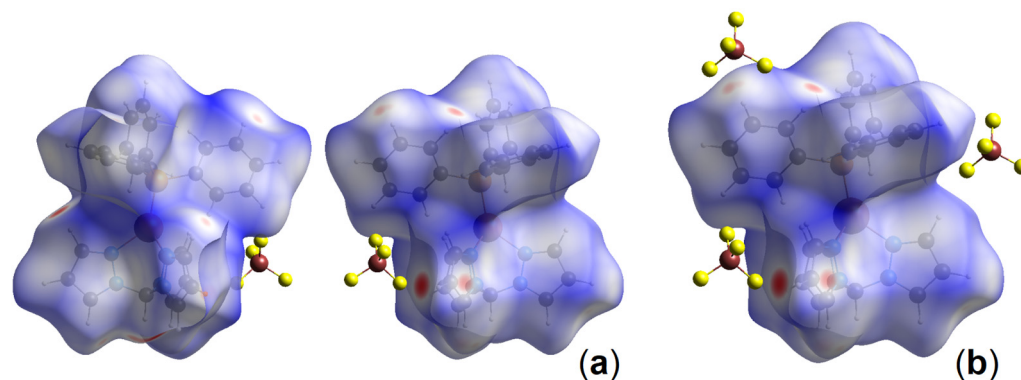

Figure 3. (**a**) Two views of the Hirshfeld surface of the $[Cu(CHpz_3)(PPh_3)]^+$ cation in the tetrafluoroborate salt mapped with d_{norm}; (**b**) Hirshfeld surface of the cation mapped with d_{norm} and drawn with the surrounding BF_4^- anions.

All the (d_i, d_e) contacts can be expressed in the form of a 2D fingerprint plot [43]. The shape of this plot, which is unique for each molecule, is determined by the dominating intermolecular contacts. The 2D fingerprint plot was constructed in this work by using reciprocal interactions, meaning that both X···Y and Y···X interactions were included in the fingerprints. The contributions of the individual interactions were also separated, and the relative percentages were assigned. In particular, Figure 4 shows the 2D fingerprint plots with the relative contributions to the Hirshfeld surface area of different pairs of atoms. As expected, van der Waals C···H (i.e., C-H···π) and H···H (i.e., π···π) close contacts provide the highest contributions, but the previously mentioned F···H close contacts are noteworthy since they represent 15% of the interactions and begin at about $1.2 + 0.9$ Å as an acute spike. Therefore, they are present only in the external face of the surface (d_e) since the tetrafluoroborate anions are out of the calculated surface, and the plot is asymmetric, with only one spike due to these interactions.

Further information from the cif file was obtained by optimizing the electronic structure using plane-wave DFT calculations. The considered real and reciprocal lattices are represented in Figure 5, together with the path connecting selected k-points of the reciprocal space. The band structure close to the valence (VB) and conduction (CB) bands is also reported in Figure 5, together with the density of states (DOS), separated by the orbital type. The occupied bands at the highest energy are mainly composed of the superposition of d-type orbitals of the Cu(I) centres, as confirmed by the DOS and by the plot of the VB. On the other hand, the unoccupied bands at the lowest energy are mainly ligand centred, with a dominant contribution of the aromatic rings of coordinated PPh$_3$ in the CB. The separation between the valence and conduction band in the reciprocal space is roughly constant, and it is around 2.8 eV.
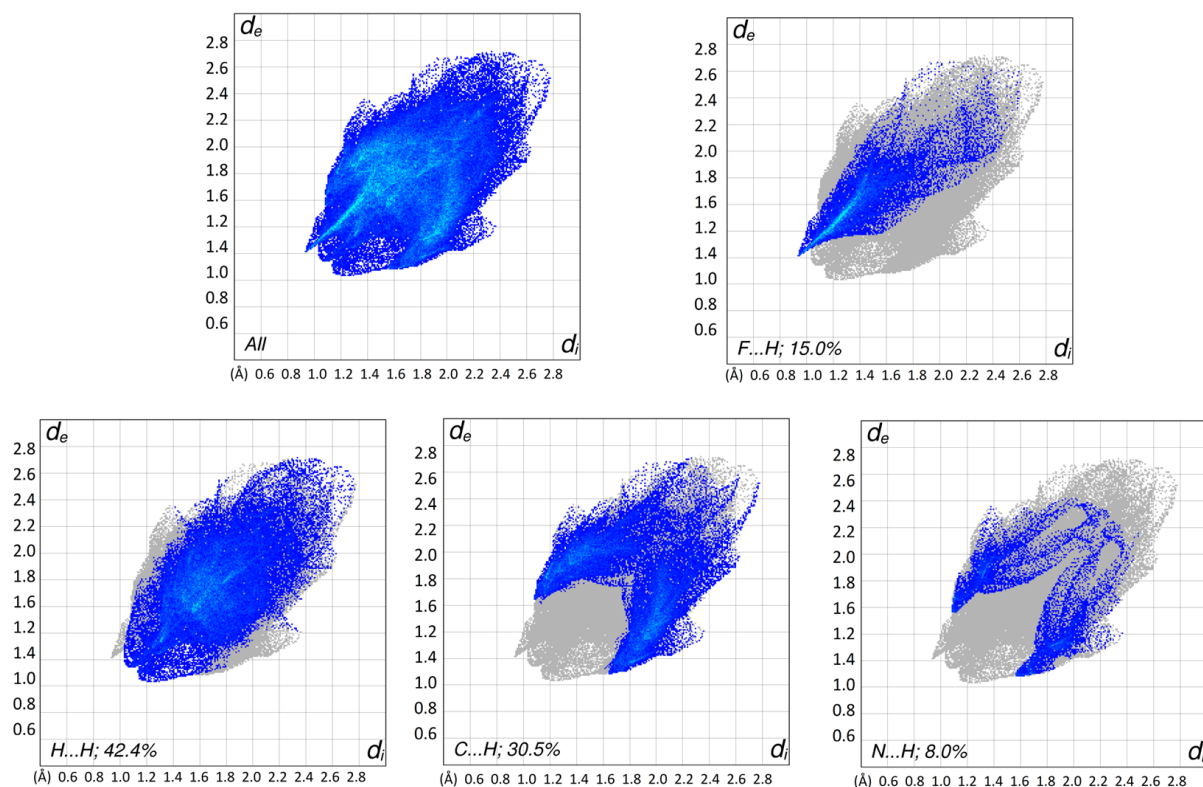
Figure 4. Two-dimensional fingerprint plots for the cation in [Cu(CHpz$_3$)(PPh$_3$)][BF$_4$].
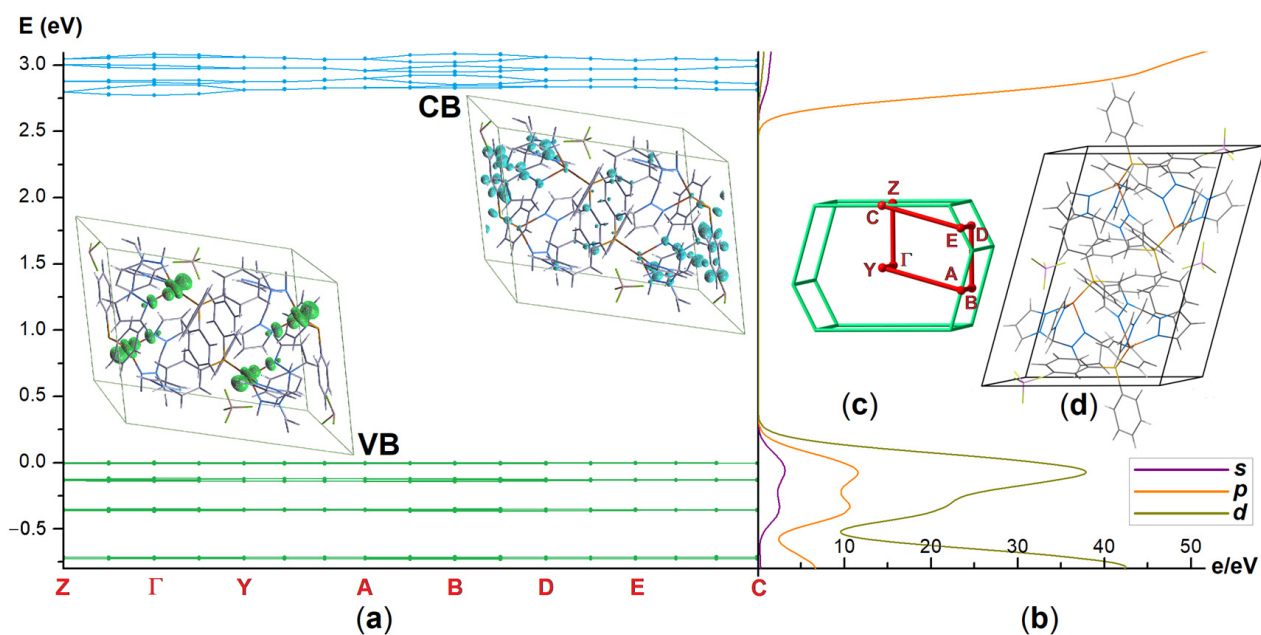

Figure 5. (**a**) Occupied (green) and empty bands (light blue) close to the VB and the CB and density plots of VB and CB (surface isovalue = 0.01 a.u.); (**b**) plot of the orbital contributions to the DOS; (**c**) reciprocal (green) lattice with path connecting selected k-points in red; (**d**) real lattice with cell content (colour map: Cu, reddish-orange; P, yellowish orange; F, greenish yellow; N, blue; C, grey; B, pink; H, white).

3.3. Fluxional Behaviour of the Complex in Solution

The ^{1}H NMR spectrum of [Cu(CHpz$_3$)(PPh$_3$)][BF$_4$] in CDCl$_3$ at 300 K shows, besides the methine proton of CHpz$_3$ at 9.44 ppm and the P-bonded aromatic rings between 7.65

and 7.40 ppm, three resonances related to the pyrazole rings at 8.43, 7.32 and 6.32 ppm. Despite the lack of equivalence of the Cu-N bonds observed in the crystal structure, the three pyrazole rings are thus equivalent in solution on the NMR timescale, indicating fluxional behaviour. Such a hypothesis is confirmed by the $^{31}P\{^1H\}$ NMR spectrum, where the single resonance of the coordinated phosphorus atom at 8.63 ppm appears broad, with full width at half maximum (FWHM) of 250 Hz (Figure 6).
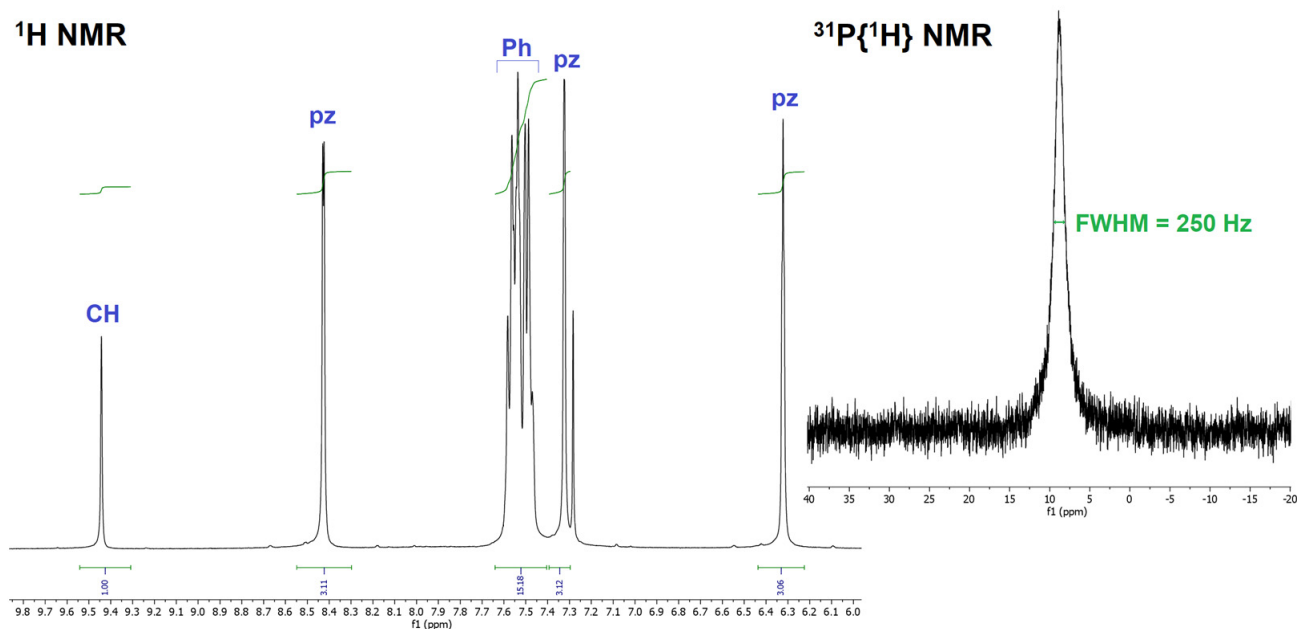

Figure 6. ^1H NMR and $^{31}P\{^1H\}$ NMR spectra of $[Cu(CHpz_3)(PPh_3)][BF_4]$ (CDCl$_3$, 300 K).

A single broad $^{31}P\{^1H\}$ NMR resonance was previously observed for the related hexafluorophosphate salt under comparable experimental conditions, but the chemical shift is slightly different (9.04 ppm). The methine ^1H resonance reported for the coordinated C-scorpionate in $[Cu(CHpz_3)(PPh_3)][PF_6]$ is also different in comparison to that of $[Cu(CHpz_3)(PPh_3)][BF_4]$, being shifted to a lower frequency by 0.3 ppm [27].

To shed light on the fluxional behaviour of the complex, the geometry was optimized by means of DFT calculations in the presence of CHCl$_3$ as continuous medium. The lack of imaginary frequencies in the simulated IR spectrum confirmed that the stationary point found is a local minimum. In the computed geometry, the BF$_4^-$ anion is much closer to the Cu(I) centre (Cu···B distance of 4.833 Å) compared to the X-ray data, where the shortest Cu···B distance is 6.213(2) Å. The anion lies between two planes defined by two pyrazole rings; thus, in the computed model, the F···H hydrogen bonds disappear, while the electrostatic interaction between the cation and anion increases. For what concerns the cation, the pyrazolyl and phenyl rings are much less staggered in the computed structure compared to the experimental one. Moreover, the Cu-N bond lengths are comprised in a reduced range, from 2.080 to 2.113 Å. The CHpz$_3$ methine carbon is less deviated from the Cu-P vector, being the computed C-Cu-P angle 172.9° (166.03(3)° in the X-ray structure). It is worth noting that the same angle was experimentally found in the X-ray structure of the nitrate salt of the complex [28]. The $\{(CHpz_3)CuP\}$ fragment is therefore more C_{3v} symmetric in the DFT-optimized geometry compared to the X-ray structure. The root mean square deviation (RMSD) between computed and X-ray geometries of the cation is 1.302 Å. The two structures are superimposed in Figure 7. Selected computed bond lengths and angles are provided in the caption of Figure 7.
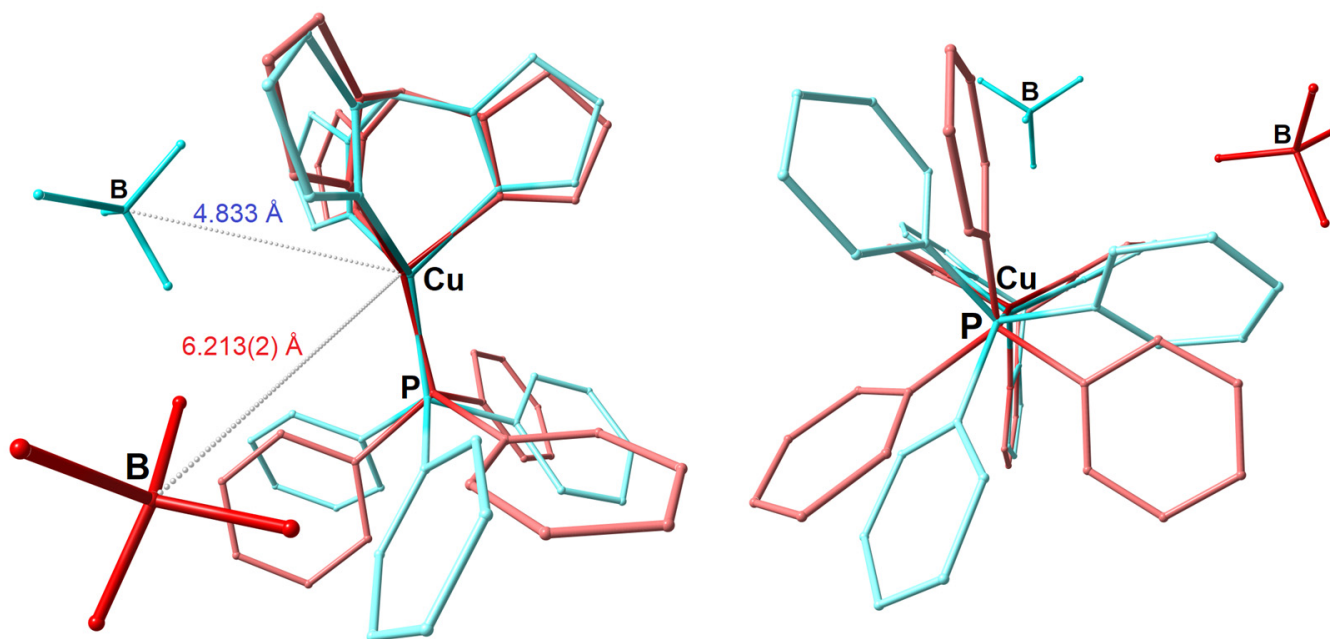
Figure 7. Two views of the DFT-optimized structure of [Cu(CHpz$_3$)(PPh$_3$)][BF$_4$] (turquoise tones) superimposed to the closest cation–anion couple found in the X-ray structure (red tones). Hydrogen atoms are omitted for clarity. Selected bond lengths [Å] and angles [°]: Cu-N, 2.080, 2.087, 2.113; Cu-P, 2.162; N-Cu-N, 87.5, 87.6, 88.8; N-Cu-P, 125.4, 125.8, 128.8.

The fluxionality of the compound was computationally investigated by employing relaxed surface scans involving the Cu-N and Cu-P bonds. The energy variations (electronic energy + nuclear repulsion) associated with the progressive elongation of the bonds are shown in Figure 8. The path related to the Cu-N dissociation is characterized by a very low energy barrier, estimated around 4.2 kcal mol^{-1}, leading to a less stable local minimum compared to the starting geometry by only 1.4 kcal mol^{-1}. The new geometry found can be described as a Cu(I) trigonal planar complex with two nitrogen and one phosphorus in the coordination sphere. One of the fluorine atoms of BF$_4^-$ is close to the trigonal plane, about 2.4 Å away from the copper atom. It is therefore likely to suppose that the anion actively participates in the fluxional behaviour, stabilizing the coordinatively unsaturated trigonal complex. The ability of tetrafluoroborate to behave as a ligand towards Cu(I) in so-called coinage (or regium) bonds is well documented in the literature [68–71]. On the other hand, Figure 8 reveals that a fluxional path involving the Cu-P bond is much less competitive.

Attempts to observe possible intermediate species involved in the fluxional behaviour were carried out by recording the ^{1}H, ^{31}P{^{1}H} and ^{19}F{^{1}H} NMR spectra at variable temperatures (Figures S3–S5), but no resonance attributable to species such as [Cu(κ^2-CHpz$_3$)(κ^2-BF$_4$)(PPh$_3$)] was clearly detected. The ^{1}H NMR spectrum maintains the symmetry of the coordinated C-scorpionate at 209 K also, with a broadening of the methine resonance upon lowering the temperature. On the other hand, the ^{31}P{^{1}H} NMR resonance becomes sharper at low temperature, whereas a weak enlargement of the ^{19}F{^{1}H} resonance was observed. It is likely to suppose that the fluxional mechanisms also remain too fast at temperatures close to the melting point of the solvent and that the relative energy of the intermediates is too high to have an appreciable concentration in solution.
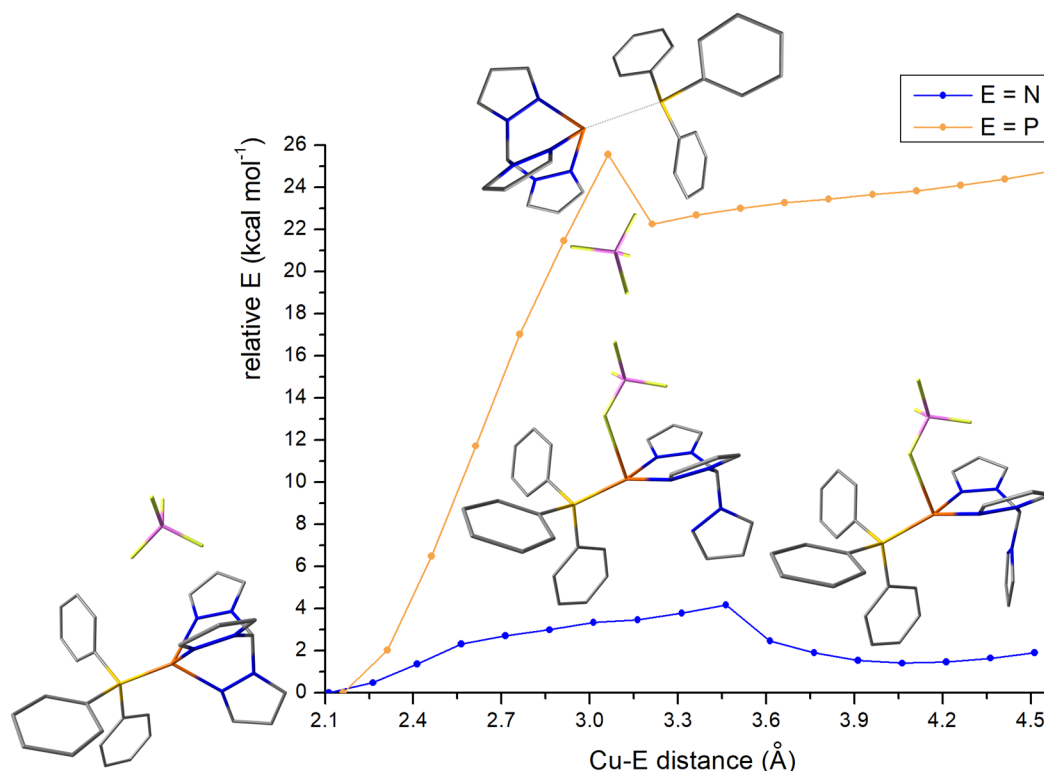
Figure 8. Relative energy profiles on varying the Cu-N (blue) and Cu-P (orange) bond distances with selected geometries. Colour map: Cu, reddish-orange; P, orange; F, greenish yellow; N, blue; C, green; B, pink. Hydrogen atoms are omitted for clarity.

4. Conclusions

The $[Cu(CHpz_3)(PPh_3)]^+$ cation represents one of the simplest examples of Cu(I) C-scorpionate derivatives. In this work, we highlighted how the geometry of the complex at the solid state is influenced by the choice of the counterion. In fact, the Cu(I) coordination sphere in $[Cu(CHpz_3)(PPh_3)][BF_4]$ is quite different compared to the previously reported nitrate salt. The intramolecular network is also deeply affected since the tetrafluoroborate anion formed several non-classical hydrogen bonds with the hydrogen atoms of the pyrazole rings. According to the DFT outcomes, the same interactions are not present in solution, but the anion plays a role in the fluxionality of the complex by establishing a regium bond with the coordinatively unsaturated metal centre obtained by the dissociation of a Cu-N bond. On considering the fields of applications for C-scorpionate complexes briefly outlined in the Section 1, the information collected in this paper appears of possible interest for the design of new Cu(I) coordination compounds with improved features.

Author Contributions: Conceptualization, M.B.; methodology, J.C. and M.B.; validation, J.C., M.B. and V.F.; formal analysis, J.C. and M.B.; investigation, J.C., M.B. and V.F.; resources, J.C., M.B. and V.F.; data curation, J.C., M.B. and V.F.; writing—original draft preparation, M.B. and J.C.; writing—review and editing, J.C., M.B. and V.F.; visualization, M.B. and J.C.; supervision, M.B.; project administration, M.B.; funding acquisition, M.B. All authors have read and agreed to the published version of the manuscript.

Data Availability Statement: Data are contained within the article and Supplementary Materials.

Conflicts of Interest: The authors declare no conflicts of interest. The funders had no role in the design of the study; in the collection, analyses or interpretation of data; in the writing of the manuscript or in the decision to publish the results.

References

1. Reger, D.L. Tris(Pyrazolyl)Methane Ligands: The Neutral Analogs of Tris(Pyrazolyl)Borate Ligands. *Comments Inorg. Chem.* **1999**, *21*, 1–28. [CrossRef]
2. Pettinari, C.; Pettinari, R. Metal derivatives of poly(pyrazolyl)alkanes I. Tris(pyrazolyl)alkanes and related systems. *Coord. Chem. Rev.* **2005**, *249*, 525–549. [CrossRef]
3. Bigmore, H.R.; Lawrence, S.C.; Mountford, P.; Tredget, C.S. Coordination, organometallic and related chemistry of tris(pyrazolyl)methane ligands. *Dalton Trans.* **2005**, 635–651. [CrossRef] [PubMed]
4. Semeniuc, R.F.; Reger, D.L. Metal Complexes of Multitopic, Third Generation Poly(pyrazolyl)-methane Ligands: Multiple Coordination Arrangements. *Eur. J. Inorg. Chem.* **2016**, *2016*, 2253–2271. [CrossRef]
5. Shakirova, O.G.; Lavrenova, L.G. Spin Crossover in New Iron(II) Coordination Compounds with Tris(pyrazol-1-yl)Methane. *Crystals* **2020**, *10*, 843. [CrossRef]
6. Martins, L.M.D.R.S.; Pombeiro, A.J.L. Water-Soluble C-Scorpionate Complexes—Catalytic and Biological Applications. *Eur. J. Inorg. Chem.* **2016**, *2016*, 2236–2252. [CrossRef]
7. McKeown, B.A.; Lee, J.P.; Mei, J.; Cundari, T.R.; Gunnoe, T.B. Transition Metal Mediated C–H Activation and Functionalization: The Role of Poly(pyrazolyl)borate and Poly(pyrazolyl)alkane Ligands. *Eur. J. Inorg. Chem.* **2016**, *2016*, 2296–2311. [CrossRef]
8. Martins, L.M.D.R.S. C-Homoscorpionate Oxydation Catalysts–Electrochemical and Catalytic Activity. *Catalysts* **2017**, *7*, 12. [CrossRef]
9. Mahmoud, A.G.; Martins, L.M.D.R.S.; Guedes da Silva, M.F.C.; Pombeiro, A.J.L. Hydrosoluble Complexes Bearing Tris(pyrazolyl)methane Sulfonate Ligands: Synthesis, Characterization and Catalytic Activity for Henry Reaction. *Catalysts* **2019**, *9*, 611. [CrossRef]
10. Cervinka, J.; Gobbo, A.; Biancalana, L.; Markova, L.; Novohradsky, V.; Guelfi, M.; Zacchini, S.; Kasparkova, J.; Brabec, V.; Marchetti, F. Ruthenium(II)–Tris-pyrazolylmethane Complexes Inhibit Cancer Cell Growth by Disrupting Mitochondrial Calcium Homeostasis. *J. Med. Chem.* **2022**, *65*, 10567–10587. [CrossRef]
11. Gobbo, A.; Pereira, S.A.P.; Biancalana, L.; Zacchini, S.; Saraiva, M.L.M.F.S.; Dyson, P.J.; Marchetti, F. Anticancer ruthenium(II) tris(pyrazolyl)methane complexes with bioactive co-ligands. *Dalton Trans.* **2022**, *51*, 17050–17063. [CrossRef]
12. Mani, F. Four-, five-, and six-co-ordinated iron(II) complexes with poly(1-pyrazolyl)methanes. *Inorg. Nucl. Chem. Lett.* **1979**, *15*, 297–302. [CrossRef]
13. Muñoz-Molina, J.M.; Belderrain, T.R.; Pérez, P.J. Group 11 tris(pyrazolyl)methane complexes: Structural features and catalytic applications. *Dalton Trans.* **2019**, *48*, 10772–10781. [CrossRef] [PubMed]
14. Humphrey, E.R.; Mann, K.L.V.; Reeves, Z.R.; Behrendt, A.; Jeffery, J.C.; Maher, J.P.; McCleverty, J.A.; Ward, M.D. Copper(II) complexes of new potentially hexadentate N_3S_3- or N_6-donor podand ligands based on the tris(pyrazolyl)borate or tris(pyrazolyl)methane core. *New J. Chem.* **1999**, *23*, 417–423. [CrossRef]
15. Mesubi, M.A.; Anumba, F.O. Coordination Chemistry of Poly(1-pyrazolyl)alkanes, Part IV. Copper(II) Complexes of Bis- and Tris-(1-pyrazolyl)methane. *Trans. Met. Chem.* **1985**, *10*, 5–8. [CrossRef]
16. Reger, D.L.; Collins, J.E.; Rheingold, A.L.; Liable-Sands, L.M. Synthesis and Characterization of Cationic [Tris(pyrazolyl)methane] copper(I) Carbonyl and Acetonitrile Complexes. *Organometallics* **1996**, *15*, 2029–2032. [CrossRef]
17. Martini, D.; Pellei, M.; Pettinari, C.; Skelton, B.W.; White, A.H. Synthesis, spectroscopic and structural characterization of Cu(II) derivatives of tris(pyrazol-1-yl)methanes. *Inorg. Chim. Acta* **2002**, *333*, 72–82. [CrossRef]
18. Melekhova, A.A.; Novikov, A.S.; Dubovtsev, A.Y.; Zolotarev, A.A.; Bokach, N.A. Tris(3,5-dimethylpyrazolyl)methane copper(I) complexes featuring one disubstituted cyanamide ligand. *Inorg. Chim. Acta* **2019**, *484*, 69–74. [CrossRef]
19. Hsu, S.C.N.; Chen, H.H.Z.; Lin, I.-J.; Liu, J.-J.; Chen, P.-Y. Dinuclear copper(I) complexes of tris(3,5-dimethylpyrazol-1-yl)methane: Synthesis, structure, and reactivity. *J. Organomet. Chem.* **2007**, *692*, 3676–3684. [CrossRef]

20. Fujisawa, K.; Tateda, A.; Miyashita, Y.; Okamoto, K.-i.; Paulat, F.; Praneeth, V.K.K.; Merkle, A.; Lehnert, N. Structural and Spectroscopic Characterization of Mononuclear Copper(I) Nitrosyl Complexes: End-on versus Side-on Coordination of NO to Copper(I). *J. Am. Chem. Soc.* **2008**, *130*, 1205–1218. [CrossRef]

21. Kujime, M.; Izumi, C.; Tomura, M.; Hada, M.; Fujii, H. Effect of a Tridentate Ligand on the Structure, Electronic Structure, and Reactivity of the Copper(I) Nitrite Complex: Role of the Conserved Three-Histidine Ligand Environment of the Type-2 Copper Site in Copper-Containing Nitrite Reductases. *J. Am. Chem. Soc.* **2008**, *130*, 6088–6098. [CrossRef]

22. Melekhova, A.A.; Novikov, A.S.; Bokach, N.A.; Avdonceva, M.S.; Kukushkin, V.Y. Characterization of Cu-ligand bonds in tris-pyrazolylmethane isocyanide copper(I) complexes based upon combined X-ray diffraction and theoretical study. *Inorg. Chim. Acta* **2016**, *450*, 140–145. [CrossRef]

23. Porchia, M.; Dolmella, A.; Gandin, V.; Marzano, C.; Pellei, M.; Peruzzo, V.; Refosco, F.; Santini, C.; Tisato, F. Neutral and charged phosphine/scorpionate copper(I) complexes: Effects of ligand assembly on their antiproliferative activity. *Eur. J. Med. Chem.* **2013**, *59*, 218–226. [CrossRef]

24. Fujisawa, K.; Noguchi, Y.; Miyashita, Y.; Okamoto, K.-i.; Lehnert, N. Mononuclear and Binuclear Copper(I) Complexes Ligated by Bis(3,5-diisopropyl-1-pyrazolyl)methane: Insight into the Fundamental Coordination Chemistry of Three-Coordinate Copper(I) Complexes with a Neutral Coligand. *Inorg. Chem.* **2007**, *46*, 10607–10623. [CrossRef]

25. Pellei, M.; Lobbia, G.G.; Santini, C.; Spagna, R.; Camalli, M.; Fedeli, D.; Falcioni, G. Synthesis, characterization and antioxidant activity of new copper(I) complexes of scorpionate and water soluble phosphane ligands. *Dalton Trans.* **2004**, 2822–2828. [CrossRef]

26. Wanke, R.; Smolenski, P.; Guedes Da Silvan, M.F.C.; Martins, L.M.D.R.S.; Pombeiro, A.J. Cu(I) complexes bearing the new sterically demanding and coordination flexible tris(3-phenyl-1-pyrazolyl)methanesulfonate ligand and the water-soluble phosphine 1,3,5-triaza-7-phosphaadamantane or related ligands. *Inorg. Chem.* **2008**, *47*, 10158–10168. [CrossRef]

27. Choi, I.Y.; Ahn, S.; Seo, J.; Park, K.-M. Synthesis and Structural Characterization of an Air-stable {[HC(pyrazolyl)$_3$]Cu(PPh$_3$)}PF$_6$. *Bull. Korean Chem. Soc.* **2004**, *25*, 1065–1067. [CrossRef]

28. Reger, D.L.; Semeniuc, R.F.; Smith, M.D. Supramolecular structures of tris(pyrazolyl)methane complexes of triphenylphosphine copper(I). *Rev. Roum. Chim.* **2002**, *47*, 1037–1046.

29. Ferraro, V.; Castro, J.; Agostinis, L.; Bortoluzzi, M. Luminescent heteroleptic copper(I) complexes with polydentate benzotriazolyl-based ligands. *Trans. Met. Chem.* **2021**, *46*, 391–402. [CrossRef]

30. Ferraro, V.; Bortoluzzi, M.; Castro, J. Synthesis of Bis(benzotriazol-1-yl)methane Derivatives by Cobalt-Catalyzed Formation of C-C Bonds. *Chem. Proc.* **2019**, *41*, 29. [CrossRef]

31. Ferraro, V.; Bortoluzzi, M.; Castro, J.; Vomiero, A.; You, S. Luminescent Cu(I) complex with bis(indazol-1-yl)phenylmethane as chelating ligand. *Inorg. Chem. Commun.* **2020**, *116*, 107894. [CrossRef]

32. Armarego, W.L.F.; Chai, C.L.L. *Purification of Laboratory Chemicals*, 5th ed.; Butterworth-Heinemann: London, UK, 2003.

33. Kubas, G.J.; Monzyk, B.; Crumblis, A.L. Tetrakis(Acetonitrile)Copper(1+) hexafluorophosphate(1-). *Inorg. Synth.* **1990**, *28*, 68–70. [CrossRef]

34. Reger, D.L.; Grattan, T.C.; Brown, K.J.; Little, C.A.; Lamba, J.J.S.; Rheingold, A.L.; Sommer, R.D. Syntheses of tris(pyrazolyl)methane ligands and {[tris(pyrazolyl)methane]Mn(CO)$_3$}SO$_3$CF$_3$ complexes: Comparison of ligand donor properties. *J. Organomet. Chem.* **2000**, *607*, 120–128. [CrossRef]

35. Bruker AXS Inc. *APEX3, SMART, SAINT*; Bruker AXS Inc.: Madison, WI, USA, 2015.

36. McArdle, P. Oscail, a program package for small-molecule single-crystal crystallography with crystal morphology prediction and molecular modelling. *J. Appl. Crystallogr.* **2017**, *50*, 320–326. [CrossRef]

37. Sheldrick, G.M. SHELXT—Integrated space-group and crystal-structure determination. *Acta Crystallogr.* **2015**, *A71*, 3–8. [CrossRef]

38. Sheldrick, G.M. Crystal structure refinement with SHELXL. *Acta Crystallogr.* **2015**, *C71*, 3–8. [CrossRef]

39. Spek, A.L. checkCIF validation ALERTS: What they mean and how to respond. *Acta Crystallogr.* **2020**, *E76*, 1–11. [CrossRef]

40. Macrae, C.F.; Bruno, I.J.; Chisholm, J.A.; Edgington, P.R.; McCabe, P.; Pidcock, E.; Rodriguez-Monge, L.; Taylor, R.; van de Streek, J.; Wood, P.A. Mercury CSD 2.0—New features for the visualization and investigation of crystal structures. *J. Appl. Crystallogr.* **2008**, *41*, 466–470. [CrossRef]

41. Spackman, P.R.; Turner, M.J.; McKinnon, J.J.; Wolff, S.K.; Grimwood, D.J.; Jayatilaka, D.; Spackman, M.A. CrystalExplorer: A program for Hirshfeld surface analysis, visualization and quantitative analysis of molecular crystals. *J. Appl. Cryst.* **2021**, *54*, 1006–1011. [CrossRef]

42. Wolff, S.K.; Grimwood, D.J.; McKinnon, J.J.; Turner, M.J.; Jayatilaka, D.; Spackman, M.A. CrystalExplorer, Version 3.1. University of Western Australia: Perth, Australia. Available online: www.crystalexplorer.net (accessed on 16 January 2024).

43. Spackman, M.A.; MacKinnon, J.J. Fingerprinting intermolecular interactions in molecular crystals. *CrystEngComm* **2002**, *4*, 378–392. [CrossRef]

44. Perdew, J.P.; Ruzsinszky, A.; Csonka, G.I.; Vydrov, O.A.; Scuseria, G.E.; Constantin, L.A.; Zhou, X.; Burke, K. Restoring the Density-Gradient Expansion for Exchange in Solids and Surfaces. *Phys. Rev. Lett.* **2008**, *100*, 136406. [CrossRef]

45. Lin, J.S.; Qteish, A.; Payne, M.C.; Heine, V. Optimized and transferable nonlocal separable ab initio pseudopotentials. *Phys. Rev. B* **1993**, *47*, 4174–4180. [CrossRef]

46. Tkatchenko, A.; Scheffler, M. Accurate Molecular Van Der Waals Interactions from Ground-State Electron Density and Free-Atom Reference Data. *Phys. Rev. Lett.* **2009**, *102*, 073005. [CrossRef]

47. Koelling, D.D.; Harmon, B.N. A technique for relativistic spin-polarised calculations. *J. Phys. C Solid State Phys.* **1977**, *10*, 3107–3114. [CrossRef]

48. Clark, S.J.; Segall, M.D.; Pickard, C.J.; Hasnip, P.J.; Probert, M.I.J.; Refson, K.; Payne, M.C. First principles methods using CASTEP. *Z. Kristallogr.* **2005**, *220*, 567–570. [CrossRef]

49. Rutter, M.J. C2x: A tool for visualisation and input preparation for Castep and other electronic structure codes. *Comput. Phys. Commun.* **2018**, *225*, 174–179. [CrossRef]

50. Hinuma, Y.; Pizzi, G.; Kumagai, Y.; Oba, F.; Tanaka, I. Band structure diagram paths based on crystallography. *Comput. Mater. Sci.* **2017**, *128*, 140–184. [CrossRef]

51. Kokalj, A. Computer graphics and graphical user interfaces as tools in simulations of matter at the atomic scale. *Comp. Mater. Sci.* **2003**, *28*, 155–168. [CrossRef]

52. Kokalj, A. XCrySDen—A new program for displaying crystalline structures and electron densities. *J. Mol. Graph. Model.* **1999**, *17*, 176–179. [CrossRef] [PubMed]

53. Grimme, S.; Hansen, A.; Ehlert, S.; Mewes, J.-M. r^{2}SCAN-3c: A "Swiss army knife" composite electronic-structure method. *J. Chem. Phys.* **2021**, *154*, 064103. [CrossRef] [PubMed]

54. Furness, J.W.; Kaplan, A.D.; Ning, J.; Perdew, J.P.; Sun, J. Accurate and Numerically Efficient r^{2}SCAN Meta-Generalized Gradient Approximation. *J. Phys. Chem. Lett.* **2020**, *11*, 8208–8215. [CrossRef] [PubMed]

55. Kruse, H.; Grimme, S. A geometrical correction for the inter- and intra-molecular basis set superposition error in Hartree-Fock and density functional theory calculations for large systems. *J. Chem. Phys.* **2012**, *136*, 154101. [CrossRef] [PubMed]

56. Caldeweyher, E.; Bannwarth, C.; Grimme, S. Extension of the D3 dispersion coefficient model. *J. Chem. Phys.* **2017**, *147*, 034112. [CrossRef] [PubMed]

57. Caldeweyher, E.; Ehlert, S.; Hansen, A.; Neugebauer, H.; Spicher, S.; Bannwarth, C.; Grimme, S. A generally applicable atomic-charge dependent London dispersion correction. *J. Chem. Phys.* **2019**, *150*, 154122. [CrossRef] [PubMed]

58. Cossi, M.; Rega, N.; Scalmani, G.; Barone, V. Energies, structures, and electronic properties of molecules in solution with the C-PCM solvation model. *J. Comput. Chem.* **2003**, *24*, 669–681. [CrossRef] [PubMed]

59. Barone, V.; Cossi, M. Quantum calculation of molecular energies and energy gradients in solution by a conductor solvent model. *J. Phys. Chem. A* **1998**, *102*, 1995–2001. [CrossRef]

60. Neese, F. The ORCA program system. *WIREs Comput. Mol. Sci.* **2012**, *2*, 73–78. [CrossRef]

61. Neese, F. Software update: The ORCA program system-Version 5.0. *WIREs Comput. Mol. Sci.* **2022**, *12*, e1606. [CrossRef]

62. Geary, W.J. The use of conductivity measurements in organic solvents for the characterisation of coordination compounds. *Coord. Chem. Rev.* **1971**, *7*, 81–122. [CrossRef]

63. Cirera, J.; Alemany, P.; Alvarez, S. Mapping the Stereochemistry and Symmetry of Tetracoordinate Transition-Metal Complexes. *Chem. Eur. J.* **2004**, *10*, 190–207. [CrossRef]

64. Alvarez, S.; Alemany, P.; Casanova, D.; Cirera, J.; Llunell, M.; Avnir, D. Shape maps and polyhedral interconversion paths in transition metal chemistry. *Coord. Chem. Rev.* **2005**, *249*, 1693–1708. [CrossRef]

65. Yang, L.; Powell, D.R.; Houser, R.P. Structural variation in copper(I) complexes with pyridylmethylamide ligands: Structural analysis with a new four-coordinate geometry index, τ_4. *Dalton Trans.* **2007**, 955–964. [CrossRef]

66. Okuniewski, A.; Rosiak, D.; Chojnacki, J.; Becker, B. Coordination polymers and molecular structures among complexes of mercury(II) halides with selected 1-benzoylthioureas. *Polyhedron* **2015**, *90*, 47–57. [CrossRef]

67. MacKinnon, J.J.; Spackman, M.A.; Mitchell, A.S. Novel tools for visualizing and exploring intermolecular interactions in molecular crystals. *Acta Crystallogr. Sect. B Struct. Sci. Cryst. Eng. Mater.* **2004**, *60*, 627–668. [CrossRef] [PubMed]

68. Legon, A.C.; Walker, N.R. What's in a name? 'Coinage-metal' non-covalent bonds and their definition. *Chem. Phys. Phys. Chem.* **2018**, *20*, 19332–19338. [CrossRef] [PubMed]

69. Dai, Y.; Zhang, Y.; Tian, J.; Liu, Z. Aquabis-(triphenyl-phosphine-*k*P)copper(I) tetrafluoridoborate. *Acta Crystallogr.* **2009**, *E65*, m1001. [CrossRef]

70. Titov, A.A.; Filippov, O.A.; Smol'yakov, A.F.; Averin, A.A.; Shubina, E.S. Copper(I) complex with BINAP and 3,5-dimethylpyrazole: Synthesis and photoluminescent properties. *Mendeleev Commun.* **2019**, *29*, 570–572. [CrossRef]

71. Ferraro, V.; Girotto, M.; Castro, J.; Bortoluzzi, M. Intense millisecond-long red luminescence from heteroleptic Cu(I) 2,1,3-benzothiadiazole complexes. *Dye. Pigment.* **2023**, *217*, 111388. [CrossRef]